JOURNAL OF SPACECRAFT AND ROCKETS
Vol. 45, No. 2, March–April 2008

Boundary-Layer Transition and Hypersonic Flight Testing

David W. Kuntz* and Donald L. Potter†
Sandia National Laboratories, Albuquerque, New Mexico 87185

DOI: 10.2514/1.29708

Boundary-layer transition continues to be a critical factor in hypersonic fight vehicle design. Measurements of transition during hypersonic flight testing provide valuable data for the development and verification of transition-prediction techniques. A summary of transition-measurement techniques used on vehicles flown by Sandia National Laboratories is presented, including sample flight data to illustrate the type of transition indication obtained from each measurement technique. The Slender Hypervelocity Aerothermodynamic Research Probe, a ballistic vehicle flown by Sandia for NASA, is used as a case study to illustrate how transition is determined for a flight vehicle and to illustrate some of the difficulties associated with these types of measurements.

I. Introduction

AN UNDERSTANDING of boundary-layer transition and its effects on flight vehicles is critical to successful hypersonic flight testing. Thermal protection system (TPS) design relies heavily on predictions of aerodynamic heating, and the large increase in aerodynamic heating that accompanies boundary-layer transition can be a significant factor in these predictions. The levels of uncertainty in transition prediction for hypersonic vehicles are quite large, and a vehicle designed with conservative transition assumptions carries excessive TPS material, whereas a vehicle designed with a nonconservative transition assumption runs the risk of thermal failure. To help reduce some of the uncertainty in transition predictions, Sandia National Laboratories has included transition instrumentation on many of its flight vehicles. Details of several types of transition instrumentation flown on hypersonic vehicles, sample measurements, and a case study of transition measurements on a ballistic flight vehicle are presented in this paper.

II. Hypersonic Flight Testing at Sandia National Laboratories

Sandia National Laboratories has been involved in hypersonic flight testing since the late 1960s and has flown more than 100 instrumented reentry vehicles. These vehicles generally consist of unique research and development tests and have included both ballistic and maneuvering vehicles with a large variety of nosetip and heat shield materials and numerous onboard experiments. Detailed analyses of these vehicles are performed before flight to predict vehicle performance and to ensure adequate design margins in both vehicle flight characteristics and thermal protection system design. The need to predict boundary-layer transition with reasonable accuracy has resulted in many of the Sandia flight vehicles being equipped with instrumentation designed to measure the onset and progression of boundary-layer transition on the vehicle surface. Data from this instrumentation have been used to evaluate transition correlations and are currently being used as benchmarks for the new generation of transition-prediction capabilities based on the parabolized stability equations. The current interest in boost-glide hypersonic vehicles, with extremely long flight times, results in an even more critical need for accurate transition-prediction capabilities and flight data with which to validate these capabilities. Thus, a thorough understanding of available transition instrumentation and its performance continues to be essential as flight tests for prototype boost-glide systems are developed.

III. Boundary-Layer-Transition Instrumentation

The changes in the flowfield surrounding a flight vehicle during boundary-layer transition can be detected with several different types of onboard instrumentation. These types of instrumentation can be divided into two basic categories: global instrumentation and local instrumentation. Global instrumentation measures the large-scale effects of transition on the vehicle, and local instrumentation measures the localized effects of transition at a particular point on the vehicle. Examples of each of these types of instrumentation, including data obtained during flight tests, are presented next.

A. Global Instrumentation

Global instrumentation is designed primarily for measuring particular aspects of flight vehicle performance. Boundary-layer transition can sometimes be detected with these devices, but the changes in vehicle performance are often subtle at transition, and confirmation with other types of devices is usually required. Two types of global instrumentation that can sometimes detect transition are flight dynamics instrumentation and base instrumentation. Flight dynamics instrumentation usually consists of onboard accelerometers, and base instrumentation typically consists of heat transfer gages and pressure transducers.

1. Flight Dynamics Instrumentation

The primary purpose of flight dynamics instrumentation is to measure the vehicle response to the flight aerodynamic environment with onboard sensors. The change in the aerodynamic environment at boundary-layer transition can sometimes be detected with these instruments. The flight dynamics instrumentation typically consists of accelerometers that measure axial acceleration and one or two components of lateral acceleration. Flight data from an axial accelerometer are shown in Fig. 1, with the time of the onset of boundary-layer transition indicated. The small changes seen in the character of the data at the time of transition are better illustrated in Fig. 2, which is the data shown in Fig. 1 with the time scale enlarged near the time of transition. Just before the indicated transition time, an increase in the high-frequency component of the signal can be seen, followed by a slight drop in the mean plotted value (an increase in the measured deceleration). These changes in the measured axial acceleration are very subtle and would likely not be identified as transition, were it not for indications from other types of instrumentation.

Presented as Paper 0308 at the 45th AIAA Aerospace Sciences Meeting and Exhibit, Reno, NV, 8–11 January 2007; received 11 January 2007; revision received 9 July 2007; accepted for publication 18 July 2007.

*Principal Member of Technical Staff, Aerosciences Department, P.O. Box 5800, Mail Stop 0825. Associate Fellow AIAA.

†Principal Member of Technical Staff, Aerosciences Department, P.O. Box 5800, Mail Stop 0825. Senior Member AIAA.

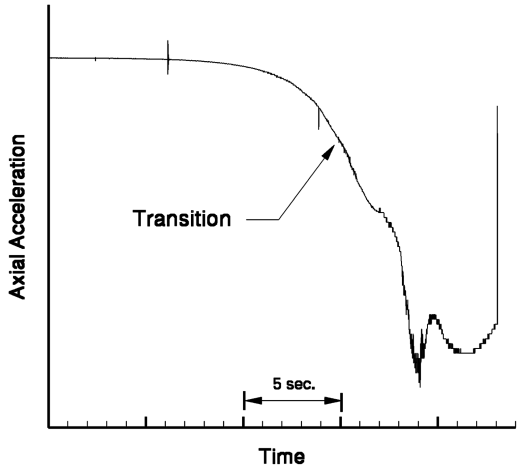

Fig. 1 Axial acceleration data.

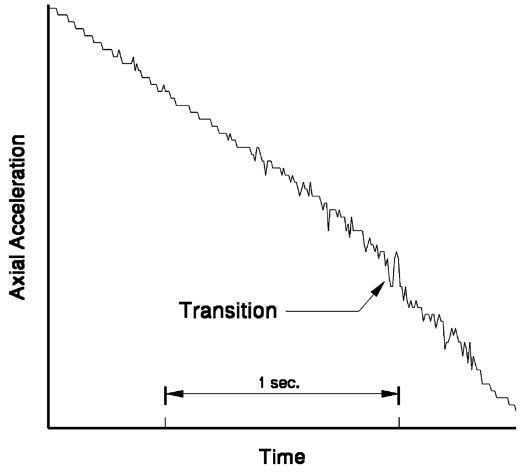

Fig. 2 Axial acceleration data with an expanded time scale near the time of boundary-layer transition.

Flight data from an accelerometer configured to measure lateral acceleration are shown in Fig. 3, with the same data shown in Fig. 4 with the time scale enlarged near the time of transition. The only indication of transition in this data is a slight increase in the high-frequency component of the signal. This subtle change in the character of the lateral acceleration data is even more difficult to detect than that seen in the axial acceleration data and further illustrates the difficulty in determining the onset of boundary-layer transition with accelerometer data.

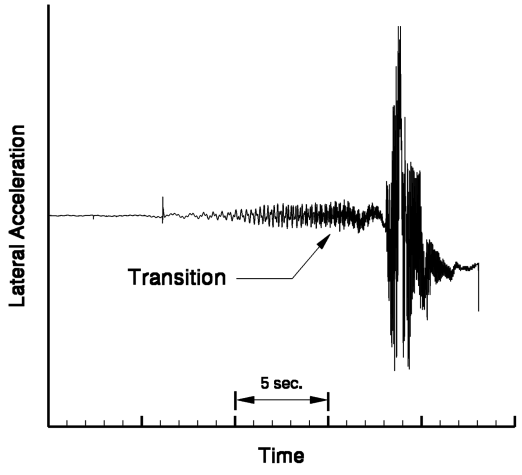

Fig. 3 Lateral acceleration data.

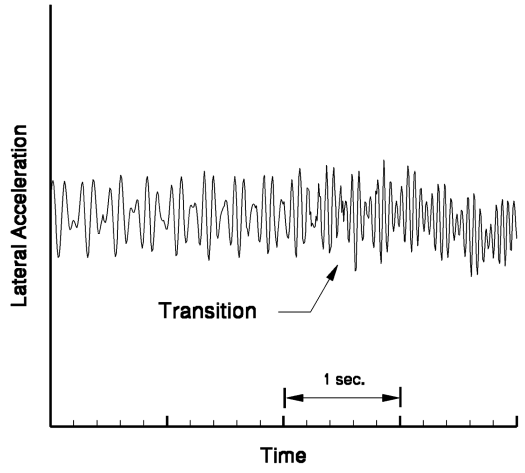

Fig. 4 Lateral acceleration data with an expanded time scale near the time of boundary-layer transition.

2. Base Instrumentation

Boundary-layer transition on a ballistic flight vehicle typically begins at the aft end of the vehicle and then proceeds forward as the vehicle descends deeper into the atmosphere and the Reynolds number gradually increases. When the boundary layer at the aft end of the vehicle transitions, the shear layers surrounding the separated base flow also become turbulent, resulting in changes in the base flowfield. Sandia flight vehicles typically contain base instrumentation primarily intended to provide base pressure and heating measurements to aid in the evaluation of analytical and computational prediction techniques. Flight vehicle base instrumentation typically consists of one or more circular-foil calorimeters and one or more pressure transducers. The effects of boundary-layer transition can sometimes be seen in these measurements.

An example of a base calorimeter measurement is shown in Fig. 5, with a close-up of the transition region shown in Fig. 6. A subtle change in the slope of the curve can be seen at the time of transition. If transition data were not available from other sources, it would be difficult to say definitively that this slope change was caused by and is indicative of transition. An example of the base pressure measurement for the same flight vehicle is shown in Fig. 7. Although the time of transition is indicated on the graph, the authors can detect no significant change in the slope of the curve, and this data illustrates the difficulty in determining transition from base measurements alone.

B. Local Instrumentation

Local instrumentation is flight vehicle instrumentation that is either intended to measure local boundary-layer transition or

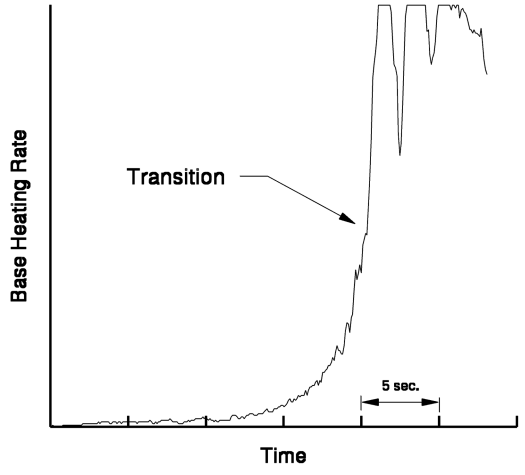

Fig. 5 Base calorimeter data.

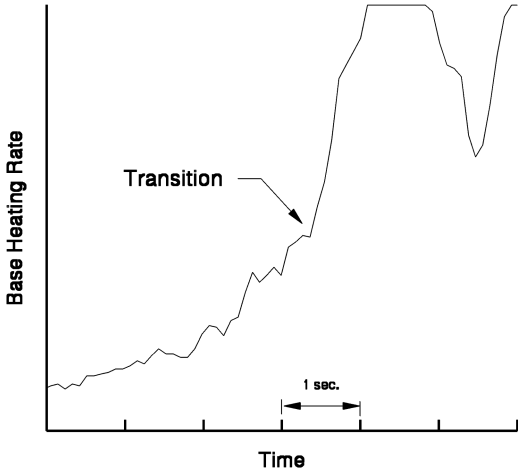

Fig. 6 Base calorimeter data with an expanded time scale near the time of boundary-layer transition.

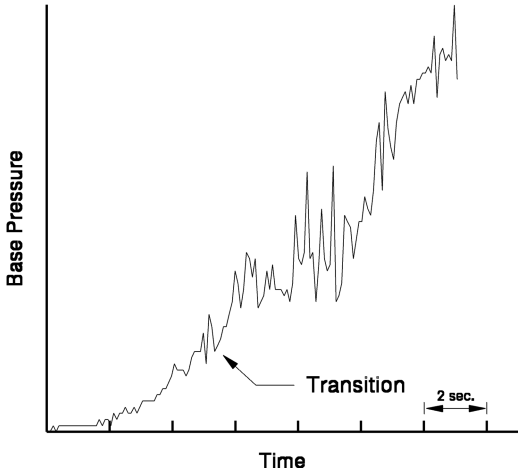

Fig. 7 Base pressure data.

measures some local property that can be directly used to determine local transition. Devices of this type are much more useful for measuring transition than global devices because they are typically much more sensitive to the changes in the flight vehicle caused by transition. If designed properly, they also have the additional benefit of being able to spatially resolve the location of transition as it progresses over the vehicle surface. Details of three types of these devices (near-surface thermocouples, photodiode transition indicators, and boundary-layer acoustic monitors) are presented next.

1. Near-Surface Thermocouples

Traditionally, the most reliable measurement device for determining local boundary-layer transition on a reentry vehicle is the near-surface thermocouple. As the name implies, this is simply a thermocouple mounted within the thermal protection system close enough to the heated surface to provide an indication of the increased heating rate associated with transition. The depth of the thermocouple nearest the surface varies, depending upon the heat shield material and the expected heating rates, and is typically chosen based on preflight analysis as a compromise between temperature and response time. A thermocouple too near the surface can exceed calibration limits before transition, and a thermocouple too far from the surface will not provide a time-accurate indication of transition. Because of the relatively high temperatures in the surface material before and immediately after transition, these thermocouples are typically type C (tungsten with 5% rhenium vs tungsten with 26% rhenium), which have a published output voltage up to a temperature

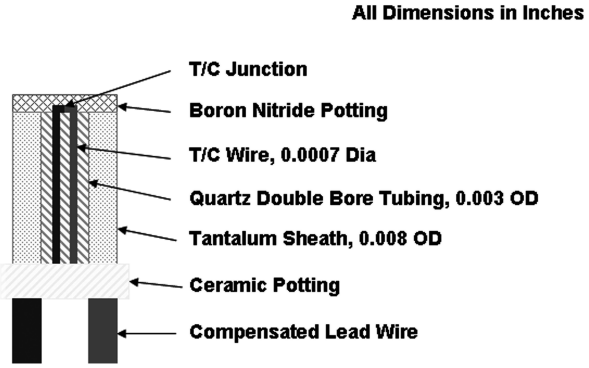

Fig. 8 Thermocouple design.

of 4660°R. To keep instrumentation errors to a minimum, these thermocouples are manufactured as small as possible. A diagram of a typical thermocouple design for transition determination is shown in Fig. 8.

To simplify installation, these thermocouples are usually installed in plugs, with up to three thermocouples installed in each plug, each at a different depth from the heated surface. The thermocouple itself is bent at a 90-deg angle near the junction before insertion into the plug. This minimizes errors due to thermal conduction down the thermocouple by aligning as much of the thermocouple as possible parallel to isotherms within the TPS material. The plug itself is epoxied into the heat shield material flush with the surface. Frequently, these plugs are then x-rayed after they are installed to obtain a final measurement of the depth of each thermocouple in the plug. Because the temperature gradient in the heat shield material can be quite large, a slight inaccuracy in thermocouple depth can produce a significant discrepancy between measured temperatures and the results of analysis codes. A diagram of a thermocouple plug (showing only a single thermocouple hole for simplicity) is shown in Fig. 9. A photograph of several thermocouple plugs (nitroxyceram, carbon phenolic, and sibalon C) is shown in Fig. 10, and a photograph of an installed thermocouple plug, viewed from the external surface, is shown in Fig. 11.

Near-surface thermocouples determine boundary-layer transition by detecting the material thermal response to the increase in heat transfer rate. This is seen as a change in the slope of the temperature-vs-time curve. Some time lag exists between the increase in heating associated with the transition phenomenon and the slope change, with the extent of lag depending upon the thermocouple depth and the properties of the material. An example of typical thermocouple measurements showing boundary-layer transition is shown in Fig. 12. Data from two thermocouples at depths of 0.025 and 0.100 in. are shown. A sharp change in the slope of the data from the near-surface thermocouple and a more gradual change in the slope of the data from the in-depth thermocouple can clearly be seen. The erratic measurements in the near-surface thermocouple shortly after transition are a result of thermocouple failure, either due to failure of the thermocouple itself resulting from high temperatures or due to ablation of the surrounding material.

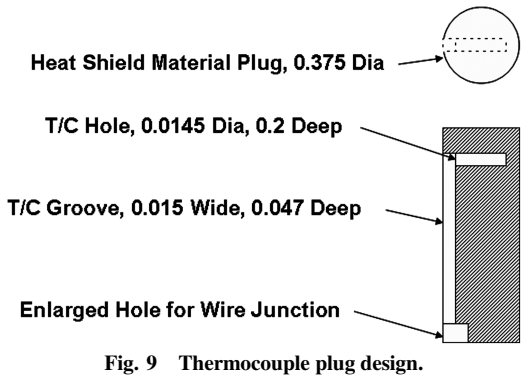

Fig. 9 Thermocouple plug design.

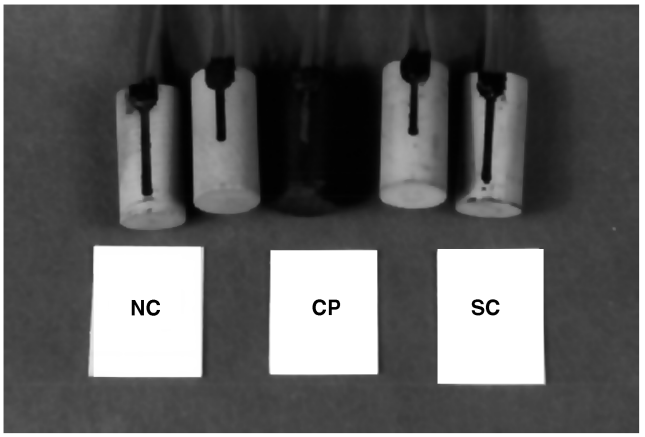

Fig. 10 Photograph of typical thermocouple plugs.

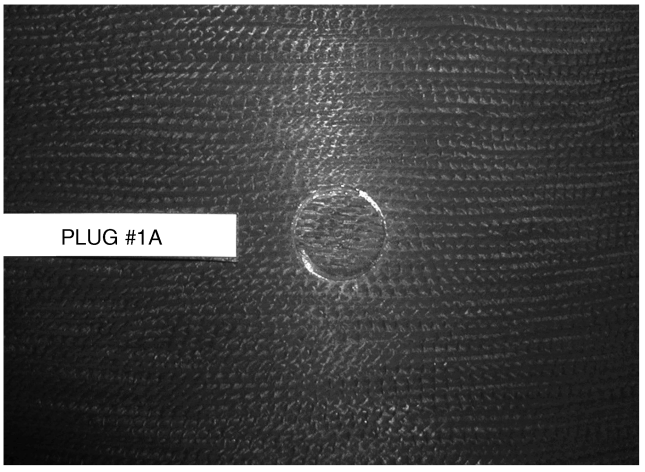

Fig. 11 Photograph of an installed thermocouple plug viewed from the surface.

2. Photodiode Transition Indictors

The photodiode transition indicator is a device that was developed at Sandia National Laboratories solely for the purpose of measuring local boundary-layer transition on a flight vehicle [1]. The concept of the device originated in the observation that the optical signature of a reentry vehicle significantly increases at boundary-layer transition, and the photodiode was an attempt to measure this increase in brightness from onboard the vehicle. The photodiode transition indicator consists of a photodiode mounted below a quartz window, which is in turn mounted flush with the external surface of a reentry vehicle. A sketch of this installation is shown in Fig. 13, and flight hardware is shown in Fig. 14. As shown in Fig. 15, the current output from the photodiode (I_T) is run through a resistor, and the voltage drop across this resistor (V_L) forms the signal that is used to determine the time of boundary-layer transition. Flight data from a photodiode transition indicator is shown in Fig. 16. The near-instantaneous rise in signal strength up to the limit of the measurement channel is obtained as boundary-layer transition moves over the quartz window.

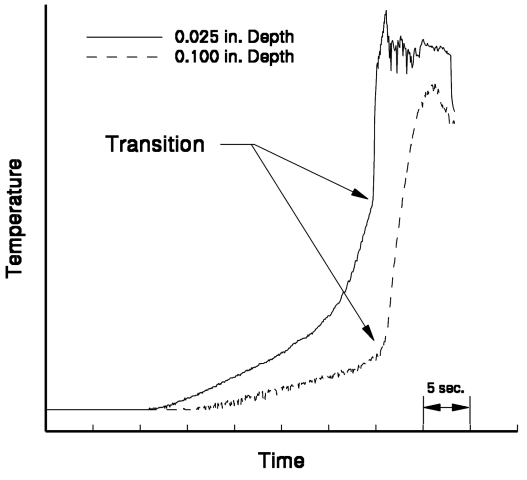

Fig. 12 Thermocouple data showing boundary-layer transition.

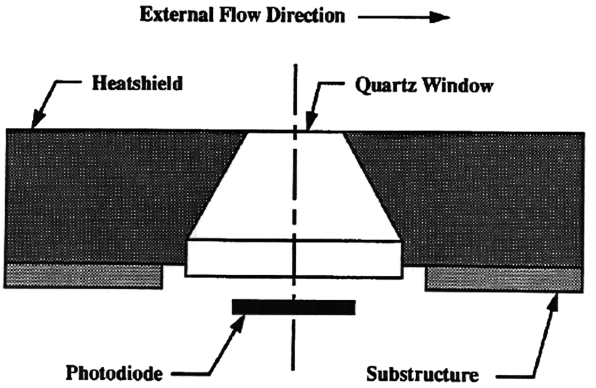

Fig. 13 Photodiode installation.

Although the inspiration for the development of the photodiode transition indicator was based on empirical evidence, the exact cause of the rise in the photodiode signal at transition was initially not known. An internally funded research project was undertaken at Sandia National Laboratories in the early 1990s to determine this cause. Four proposed signal sources were investigated:

1) The temperature of the surface of the quartz window rises rapidly at boundary-layer transition due to the near-instantaneous rise in heating rate. It was proposed that the associated rapid rise in temperature results in the quartz material emitting in a portion of the electromagnetic spectrum that is within the spectral response of the photodiode.

2) The relatively low thermal conductivity of the heat shield results in its surface temperature rising extremely rapidly at boundary-layer transition to an ablation temperature of approximately 6000°R. Although the quartz window is surrounded by a thin layer of epoxy,

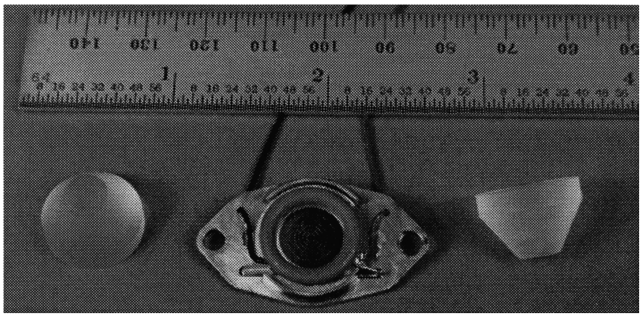

Fig. 14 Photodiode hardware.

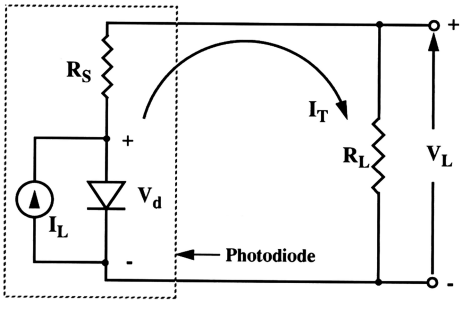

Fig. 15 Photodiode equivalent circuit.

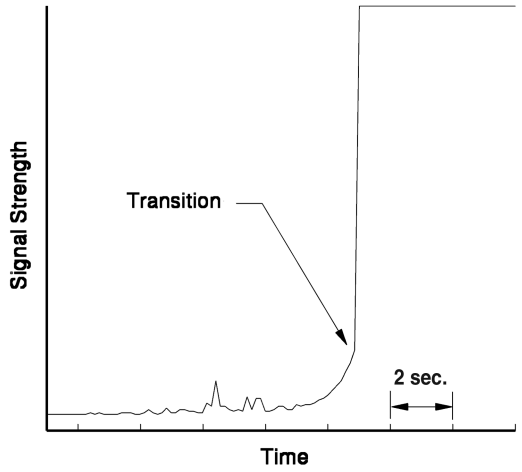

Fig. 16 Photodiode data showing boundary-layer transition.

the epoxy fails at a temperature of approximately 1000°R, and the heat shield material, at high temperatures, expands to fill any gap between the heat shield and the quartz left by the failed epoxy. The relatively high emissivity of the heat shield material and its high ablation temperature indicate that radiation from the heat shield through the edges of the quartz window to the photodiode could be the cause of the sudden change in photodiode signal observed at boundary-layer transition.

3) The thickness, temperature, and chemical composition of the boundary layer can change significantly when transition occurs, and it was proposed that radiative emissions from the gasses within the boundary layer could change significantly at transition, causing the photodiode signal.

4) The increase in heating rate associated with boundary-layer transition results in an increase in surface ablation and thus an increase in ablation products in boundary-layer adjacent to the quartz window. It was proposed that these ablation products, both in the form of carbon compounds produced by chemical reactions between the carbon and the high-temperature gases in the boundary layer and in the form of solid carbon particles that have broken away from the nosetip or heat shield and are entrained within the gases near the surface of the vehicle, could be emitting in a wavelength visible to the photodiode.

The results of this investigation indicated that of these four proposed signal sources, only radiation from the heat shield material bordering the quartz window produced sufficient signal strength to account for the flight data. Thus, like the near-surface thermocouples, the photodiode is reacting to the increase in the temperature of the surface of the heat shield material at transition and is, in effect, serving as a highly nonlinear surface-temperature measuring device. Unfortunately, the photodiodes used in these devices in the past are no longer available, and some development work with currently available components would be necessary to produce a photodiode transition indicator for current flight vehicles. The results of the preceding investigation could be used to simplify the design process to produce a new device, significantly reducing the uncertainties that were present in the original photodiode design. Additional details of these devices and the investigations of the signal source can be found in [2].

3. Boundary-Layer Acoustic Monitors

The high-frequency pressure fluctuations produced in a turbulent boundary layer can be detected by local onboard sensors that are usually referred to as boundary-layer acoustic monitors, or BLAMs. At Sandia National Laboratories, BLAMs have taken two different forms. The first, and simplest, is a microphone that is attached to the rear surface of the heat shield material. The significant increase in acoustic signal as the boundary transitions in the vicinity of the microphone produces a time-accurate indication of transition.

The second form of BLAM used at Sandia makes use of the transducers intended to measure surface ablation. Sandia has developed and flown a number of acoustic recession gages for measuring the surface recession of nosetips, antenna windows, and control surfaces during flight. These devices use acoustic transducers to produce an acoustic signal in the material that moves through the material, reflects off the ablating surface, and returns to the transducer. The "time of flight" of the acoustic signal, corrected for the effects of temperature on sound speed in the material, can be used to determine the near-instantaneous thickness of the material. A photograph of acoustic-recession-gage flight hardware, including an instrumented nosetip and instrumented antenna windows, is shown in Fig. 17. In addition to transmitting and receiving the reflected acoustic signal, the transducers used in these devices can be used to measure the ambient noise and thus can be used as a BLAM. An example of a transition measurement made with an acoustic-recession-gage transducer is shown in Fig. 18.

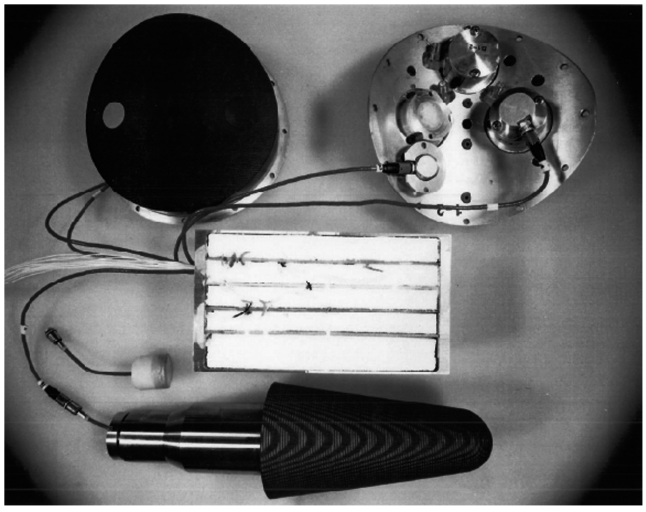

Fig. 17 Acoustic recession gage hardware.

Boundary-layer acoustic monitors rely on the conduction of acoustic energy from the aerodynamic surface to the measurement device. If a localized transition measurement is desired, care must be taken to ensure that the devices are receiving an acoustic signal from the measurement location only and not from some other portion of the flight vehicle. Typical ballistic reentry vehicle heat shields are made of carbon phenolic by wrapping a phenolic-impregnated carbon tape around a conic mandrel. The tape lies at an angle relative to the surface, producing no long acoustic paths through carbon fibers to other portions of the vehicle. The new generation of heat shields made of large sections of carbon fabric could conceivably result in long continuous acoustic paths through the carbon fibers within the material. If BLAMs are to be used to determine transition on vehicles made with these new materials, care will have to be taken

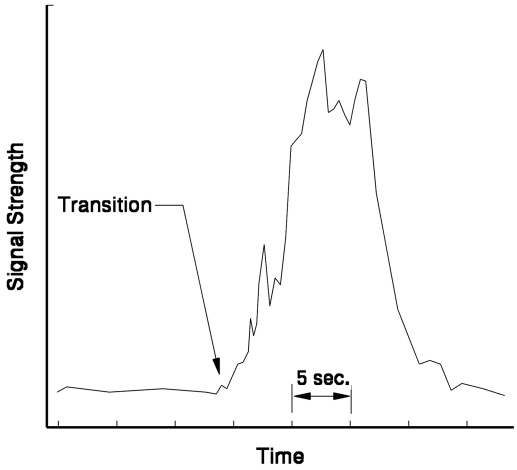

Fig. 18 BLAM data showing boundary-layer transition.

to ensure that localized measurements of transition are produced by these devices.

IV. Transition Case Study: SHARP-B2

To better illustrate how flight data is used to determine boundary-layer transition on a vehicle, a case study of a ballistic flight is presented. The particular case study presented is the second ballistic vehicle flown as part of the Slender Hypervelocity Aerothermodynamic Research Probes (SHARP) program [3], SHARP-B2. This vehicle was chosen not because of the quality of the data, but rather because the particular nature of this flight eliminates the classification issues that prevent most flight data from being published in an open forum. The SHARP program was initiated to test NASA Ames Research Center's ultra-high-temperature ceramics (UHTC) materials that were under development with the goal of enabling sharp leading edges for future space vehicles.

A photograph of the SHARP-B2 flight vehicle is shown in Fig. 19. The vehicle was a slender sphere-cone equipped with four strakes, 5.121 in. in length, located 38.807 in. from the nosetip. Each of these strakes was composed of three different UHTC materials and was mounted on a mechanism that enabled it to be rotated into the vehicle during the flight after it had been exposed to the desired level of reentry heating. A photograph of one of the strakes and its mounting mechanism is shown in Fig. 20.

The SHARP-B2 vehicle was equipped with a parachute recovery system intended to decelerate the vehicle to a relatively low velocity before water entry. Unfortunately, at deployment, the parachute separated from the vehicle, resulting in a higher-than-desired water-impact velocity. Although the vehicle broke up at water entry, the strakes and major vehicle components were recovered intact, allowing for postflight examination of the experiments. A graphic shown in Fig. 21 indicates the planned sequence of events for the flight.

A. Transition Instrumentation

The primary goal of the SHARP B-2 flight test was to expose the strakes to known levels of reentry heating. The strakes were to be retracted before the expected boundary-layer transition time, and thus measurement of transition was considered a secondary objective. As a result, the transition instrumentation on SHARP-B2 was limited to near-surface thermocouples located at four axial stations and two meridional angles. A total of eight thermocouple plugs were installed in the heat shield, four containing one type-C thermocouple at a depth of 0.025 in. and four containing three type-K thermocouples at depths of 0.025, 0.063, and 0.100 in. Details of the thermocouple plugs, including their locations, are included in Table 1. The primary purpose of the thermocouple plugs located at the 39.014- and 43.900-in. stations was to provide temperatures to help quantify the aerothermal environment that the strakes were exposed to before their retraction. Thus, the thermocouples in these plugs were type-K, which have a lower maximum temperature than type-C thermocouples, but provide higher-resolution measurements. Fortunately, these thermocouples survived to transition and thus also provided useful transition data. The thermocouple plugs located at the 22.003- and 60.942-in. stations were intended to measure boundary-layer transition, but total vehicle instrumentation constraints limited these plugs to a single thermocouple each.

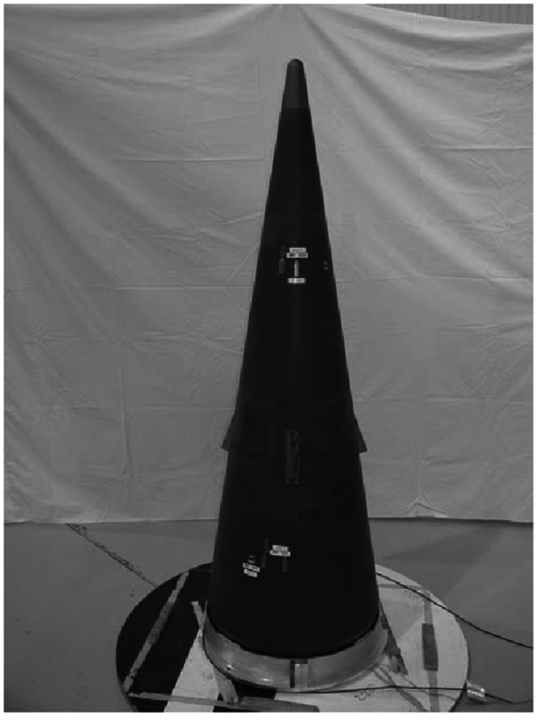

Fig. 19 Photograph of the SHARP-B2 flight vehicle.

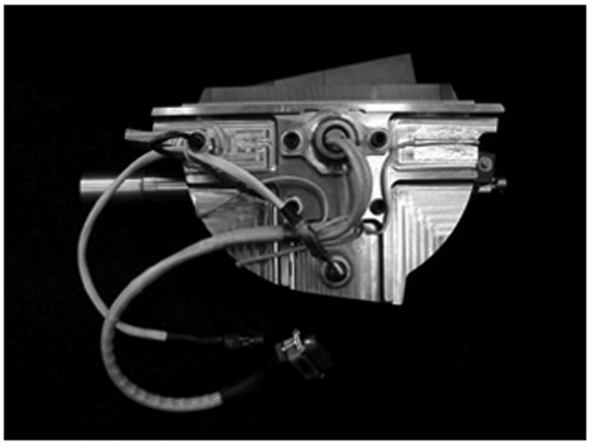

Fig. 20 Photograph of one strake and mounting hardware.

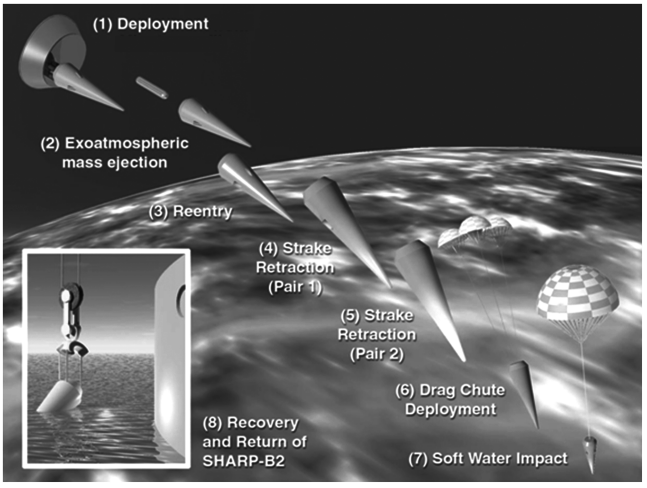

Fig. 21 SHARP-B2 intended sequence of events.

B. SHARP-B2 Flight Data Reentry

Flight vehicles rarely perform completely as expected, and SHARP-B2 was no exception. The flight was nominal through retraction of the first set of strakes, which occurred at a relative time of approximately 6.7 s. Unfortunately, one of the second set of strakes (located on the 288-deg meridional angle) failed to retract properly and was in a partially retracted position for approximately 6.6 s before retracting completely (from 8.4 to 15.0 s). This caused the vehicle to experience a significant angle-of-attack oscillation during the time of boundary-layer transition, which can be seen in the thermocouple data.

Table 1 SHARP-B2 thermocouple locations and indicated transition times

Plug axial location, in.	Plug meridional location, deg	Thermocouple type	Thermocouple depth(s), in.	Transition indication, s
22.003	153	C	0.025	12.8–13.1
22.003	333	C	0.025	12.2–12.4
60.942	153	C	0.025	9.8–10.1
60.942	333	C	0.025	12.2–12.4
39.014	153	K	0.025 0.063 0.100	9.8–10.0 13.0–13.1
39.014	333	K	0.025 0.063 0.100	12.2–12.4
43.900	153	K	0.025 0.063 0.100	9.9–10.2 13.0–13.1
43.900	333	K	0.025 0.063 0.100	12.2–12.4

The thermocouple data for the eight thermocouple plugs is presented in Figs. 22–27. Spurious data points that occurred in nearly all thermocouple channels at relative times of approximately 12.6 and 12.8 s have been removed for clarity. In addition to the flight data, the results of laminar calculations are presented to illustrate the sudden change in the slope of the temperature curves at transition, above that typically seen during the laminar portion of the flight. These calculations were made using the 2IT/SANDIAC/HIBLARG [4–7] suite of codes to determine heating, and the charring material ablation (CMA) [8] code to determine material thermal response. The 2IT/SANDIAC/HIBLARG codes use an inviscid/integral boundary-layer technique to compute the appropriate boundary conditions for the industry-standard CMA, a one-dimensional ablation code. Unfortunately, no angle-of-attack data were available for the computations, and thus these results are presented for the zero angle-of-attack case and show no indication of the oscillatory nature of the flight data. Also, laminar calculations using these techniques historically tend to be somewhat conservative, and thus the computed laminar temperatures are generally higher than the flight data before transition.

The thermocouple data near the time of boundary-layer transition for the two type-C thermocouples located at the 22.003-in. station are presented in Fig. 22. The effects of the angle-of-attack oscillation can be seen in the data as a sinusoidal temperature oscillation superimposed over the steadily rising mean temperatures. The sudden changes in the rate of change of temperature can be seen at boundary-layer transition, with thermocouple failure seen shortly thereafter. By comparing the two curves in this figure, it can be seen that the sinusoidal temperature oscillations are out of phase, because the thermocouples are on the opposite sides of the vehicle. It is also interesting to note that in both cases, it appears that the boundary

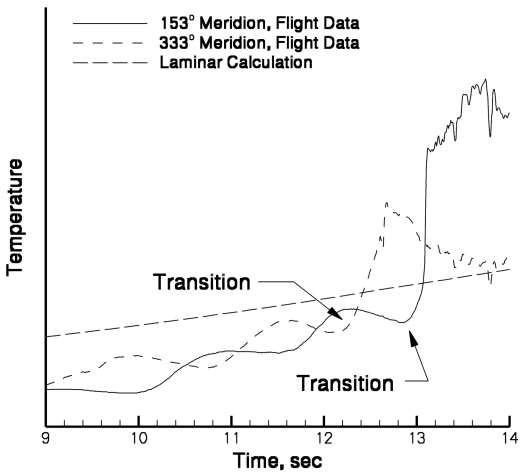

Fig. 22 Thermocouple data, 22.003-in. station.

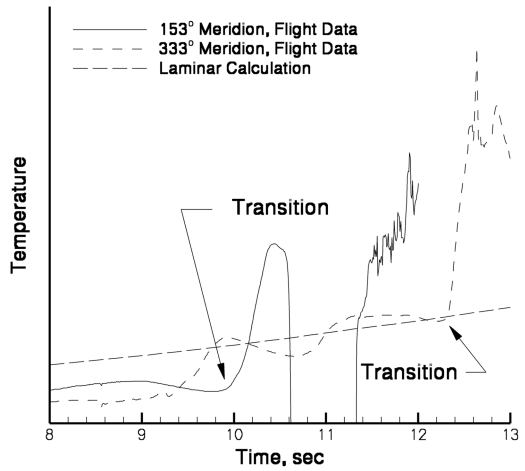

Fig. 23 Thermocouple data, 60.942-in. station (153-deg meridion data removed after thermocouple failure for clarity).

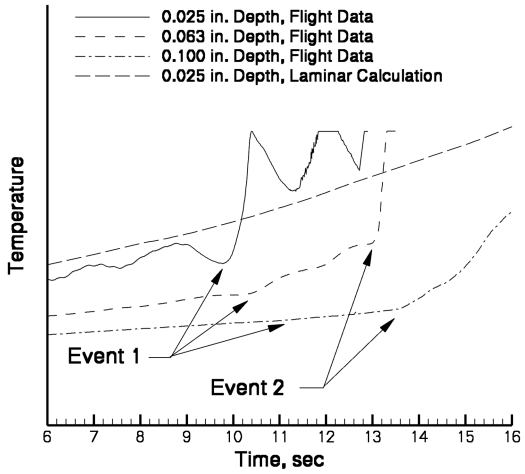

Fig. 24 Thermocouple data, 39.014-in. station, 153-deg meridion (data removed after thermocouple failure for clarity).

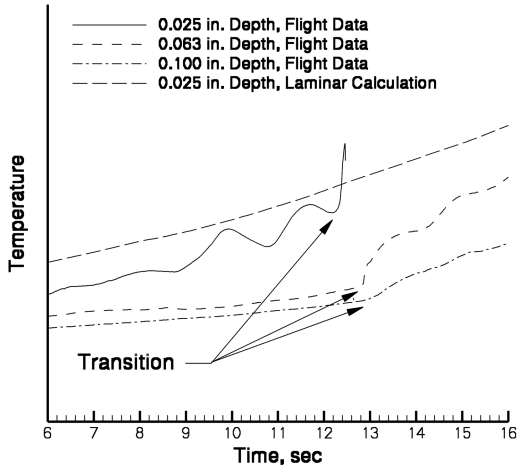

Fig. 25 Thermocouple data, 39.014-in. station, 333-deg meridion (data removed after thermocouple failure for clarity).

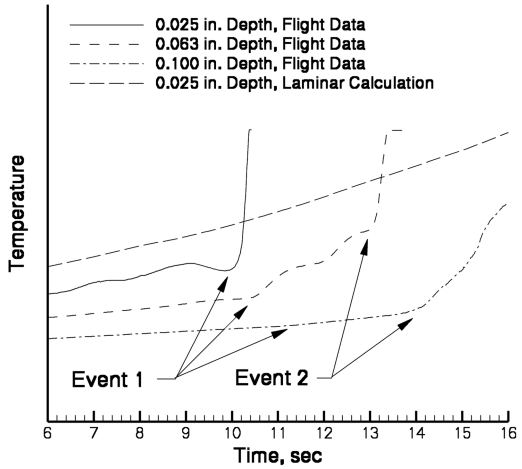

Fig. 26 Thermocouple data, 43.900-in. station, 153-deg meridion (data removed after thermocouple failure for clarity).

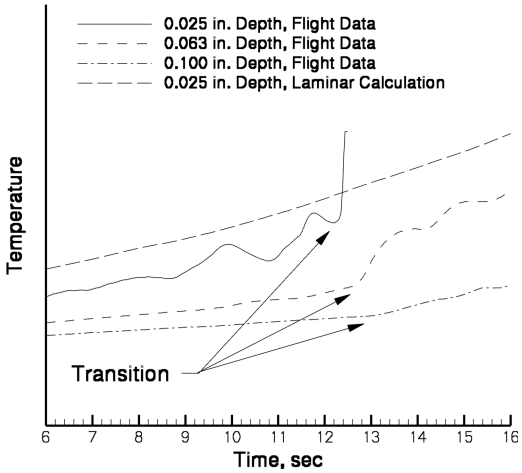

Fig. 27 Thermocouple data, 43.900-in. station, 333-deg meridion (data removed after thermocouple failure for clarity).

layer transitioned when that point was on the leeward side of the vehicle.

The thermocouple data near the time of boundary-layer transition for the two type-C thermocouples located at the 60.942-in. station are presented in Fig. 23. The trends seen in this data are similar to those seen in the 22.003-in. data, except that the 153-deg meridian location appears to transition when it first goes leeward, whereas the 333-deg meridian location appears to remain laminar for approximately two cycles of the angle-of-attack oscillation before it transitions.

The thermocouple data near the time of boundary-layer transition for the four thermocouple plugs in the vicinity of the strakes are presented in Figs. 24–27. Each figure contains the data from the three thermocouples located in a single plug, plus the laminar calculation results. The temperature data for the 39.014- and 43.900-in. stations on the 333-deg meridian (shown in Figs. 25 and 27, respectively) provide a clear indication of transition. It can be seen in these figures that as the depth of the thermocouple in the plug increases, the magnitude of the change in slope of the curve decreases and the lag in the transition indication increases.

The temperature data for the 39.014- and 43.900-in. stations on the 153-deg meridian (shown in Figs. 24 and 26, respectively) provide an indication of two separate events that resulted in a significant increase in the slope of the temperature curves. These two events, separated by approximately 3 s, both appear to have significantly increased the heating rate to the vehicle surface and, similar to the single-transition events seen in the other thermocouple data, appear to have occurred as this point on the vehicle was leeward. To the authors' knowledge, this dual event has not been reported in prior flight tests and is unique to the SHARP-B2 vehicle. The exact cause of this phenomenon is not known, but a possible explanation is that the local flow, significantly influenced by the oscillating angle of attack, became transitional at the initial event and remained in this state for several seconds before becoming fully turbulent at the second event. Unfortunately, no additional transition information is available from any other instrumentation on this vehicle, and thus the exact cause of this double event may never be known.

A summary of all the transition information for SHARP-B2 is included in Table 1 and presented graphically in Fig. 28. Figures of this type are very useful because they present all the transition information on a single plot and allow trends in axial location, meridional angle, and time to be clearly seen. The length of the bar in this figure is an indication of the uncertainty in the transition time, and the data are arranged along the vertical axis so that the higher the bar is on the graph, the further aft the sensor is on the vehicle. Thus, the typical trend of transition to move forward on the vehicle with time is seen as a general downward-and-to-the-right trend in the locations of the bars. It can be seen in this figure that no such trend existed for the transition on SHARP-B2. The relatively large angle-of-attack oscillations appear to have had a significant effect on transition. The first events that occurred at the midstations on the 153-deg meridian are nearly simultaneous with the transition indication obtained at the aft station at that same meridional angle. This is consistent with the beginning of transition occurring halfway down the body at this first event, with the flow becoming fully turbulent by the aft station. Transition at the forwardmost station on this meridional angle is consistent with the second events that occurred at the vehicle midstation, indicating that the midstation

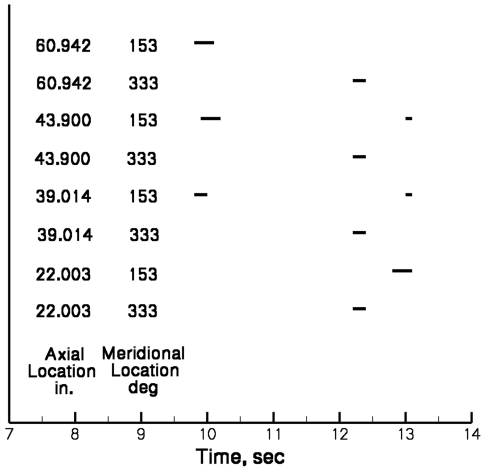

Fig. 28 SHARP-B2 transition summary.

transitioned completely at the same time the forward part of the vehicle transitioned. On the opposite side of the vehicle, on the 333-deg meridian, the flow appears to have transitioned simultaneously: again, most likely, a result of the large angle-of-attack oscillations.

V. Conclusions

Several different types of boundary-layer transition instrumentation are available with which to measure the onset and progression of transition on a hypersonic flight vehicle. Global devices such as accelerometers, base pressure transducers, and base heat flux gages can provide an indication of the effects of transition on total vehicle performance. However, the effects of transition on the measurements from these devices are often subtle, and confirmation from other data sources is frequently necessary to interpret these measurements properly. Local devices such as near-surface thermocouples, photodiode transition indicators, and boundary-layer acoustic monitors can measure the local effects of transition at specific points on the vehicle and thus offer the most reliable measurement of the onset and progression of transition. However, as seen in the SHARP-B2 data, even local devices can produce measurements that are difficult to interpret, and all available data concerning the flight of a vehicle must be used in the determination of boundary-layer transition. As new generations of flight vehicles are developed, transition data from flight tests will continue to be important in the development and verification of transition-prediction techniques, techniques that will play a critical roll in the successful design of the new thermal protection systems.

Acknowledgments

The authors wish to thank Terry Jordan-Culler, Basil Hassan, and David Keese for their help in the preparation of this document.

References

[1] Blodgett, S. R., Conrad, B. T., Shrock, K. W., Wilken, A. C., Sterk, M. W., and Chaffin, R. J., "A Novel Reentry Vehicle Instrument—The Photodiode," *ISO Transactions*, Vol. 26, No. 3, July 1987, pp. 19–23.

[2] Kuntz, D. W., Wilken, A. C., and Payne, J. L., "Analysis of the Photodiode Boundary Layer Transition Indicator," *Journal of Thermophysics and Heat Transfer*, Vol. 9, No. 3, July–Sept. 1995, pp. 499–507.

[3] Loomis, M., and Palmer, G., "Pre-Flight CFD Analysis of Arc Jet and Flight Environments for the SHARP-B2 Flight Experiment," 39th AIAA Aerospace Sciences Meeting and Exhibit, Reno, NV, AIAA Paper 2001-0982, Jan. 2001.

[4] Daywitt, J., Brant, D., and Bosworth, F., *Computational Technique for Three-Dimensional Inviscid Flow Fields About Reentry Vehicles*, General Electric, Philadelphia, Apr. 1978.

[5] Noack, R. W., and Lopez, A. R., "Inviscid Flow Field Analysis of Complex Reentry Vehicles, Volume 1: Description of Numerical Methods," Sandia National Labs. Rept. SAND-87-0776/1, Albuquerque, NM, Oct. 1988.

[6] Noack, R. W., and Lopez, A. R., "Inviscid Flow Field Analysis of Complex Reentry Vehicles, Volume 2: User's Manual," Sandia National Labs. Rept. SAND-87-0776/2, Albuquerque, NM, Nov. 1988.

[7] Polansky, G. F., "Hypersonic Integral Boundary Layer Analysis of Reentry Geometries (HIBLARG) Code Description and User's Manual Version 2.0," Sandia National Labs. Rept. SAND-89-0552, Albuquerque, NM, Mar. 1990.

[8] Lauger, L. M., Kaestner, P. C., and Blackwell, B. F., "Operation Instructions for Charring Material Ablation Code," Sandia National Labs., Rept. SLA-73-0745, Albuquerque, NM, 1973.

R. Kimmel
Associate Editor